Chapter 4

Novolac resin-based network with aminopyridine units for the removal of azo dyes from aqueous solutions

4.1 Introduction

Contamination of receiving water streams with azo dye colorants is a problematic issue to the ecosystem of aquatic life and human beings. Discharge of untreated colored effluents from different dyestuff manufacturing and using industries into the neighboring water bodies is ultimately linked to pollution of receiving water bodies of general population use. In the worst scenario, some of the azo dyes and their degradation products can be toxic, mutagenic or carcinogenic. Therefore, removal of these colored compounds from effluent streams is a task of top priority before discharge to the environment. Amongst various techniques for dyes removal, adsorption has become an attractive option because of its simple operation, efficacy and economic feasibility. In recent decades, polymeric adsorbents have evoked a lot of interest because they offer noteworthy features. *Chapter-1* vividly addressed azo dye contamination, toxicity, removal techniques including adsorption and literature review on polymer-based adsorbing materials in azo-dye wastewater decontamination. *Chapter-1* further indicated fascinating attributes to phenolic resins desirable for immense applications in many industrial fields. The growing interest on the utilization of novolac type phenolic resin in the design of dye adsorbing sorbent materials as addressed in *Chapters-2* and *3* indicates that potential of such resin is still little explored in

the design of polymeric adsorbents and yet to be addressed. Crosslinkable novolac epoxy resin as reported in *Chapter-2* is easy to manipulate for such application and seems to provide further credence to develop varieties of novolac-based network materials by incorporating various amines. As an extension in this research direction, this chapter focuses on the design of pyridine-rich novolac-based network along with key findings on azo dye adsorptive removal performance. To the best of our knowledge, no literature is available on azo dye removal by such material.

4.2 Objective

This chapter aims to describe the synthesis of novolac-based network material **4.1** consisting of 3-aminopyridine units for adsorptive removal of a variety of azo dyes, i.e., methyl orange (MO), orange II (OII) and orange-G (OG) from aqueous solution.

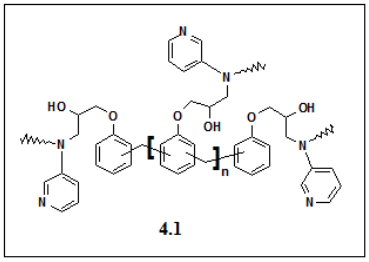

Figure 4.1. 3-aminopyridine rich novolac-based network **4.1**

4.3 Experimental Section

4.3.1 Materials and Measurements

Chemicals were purchased and used without purification. NMR spectrum was recorded on DELTA2 NMR spectrometer. FTIR spectra were recorded on Perkin Elmer spectrophotometer using KBr discs. Particle size and particle size distribution was determined using Particle size analyser (Model: Helos (H1004) & Sucell). TGA analysis was conducted with Perkin Elmer STA 6000 instrument under nitrogen atmosphere. Elemental analysis was performed by CHN/S/O Analyzer (Perkin Elmer, Series II, 2400). Surface morphology of polymer network was examined by field emission scanning electron microscopy (FE-SEM; Carl Zeiss Supra 55). Brunauer-Emmette-Teller (BET)[1] surface area analysis was carried out using ASAP 2020 Micrometrics instrument under nitrogen environment. Degasification of the network sample was done at 350 °C for 6 h before analysis. UV-vis spectra were recorded on Shimadzu UV-1800 spectrophotometer. A pH meter (Tosniwall, CL 46) was employed for the pH measurements.

4.3.2 Synthesis of novolac resin 2.1

The synthesis was described in *Chapter-2.*

4.3.3 Synthesis of novolac epoxy resin 2.2

Novolac epoxy resin **2.2** was obtained by using the method described in *Chapter-2*.

4.3.4 Synthesis of novolac-based network 4.1

Novolac-based epoxy resin **2.2** (0.45g) and 3-aminopyridine (0.169 g, 1.8 mmol) were mixed in dichloromethane to obtain a clear solution. After removing solvent, the mixture was allowed to react for 5h at 95-100^{o}C with stirring in bulk. The solid product was separated. After cooling to room temperature, the obtained solid was washed two times using 1,4-dioxan and then kept overnight in DMSO. After that, the solid was filtered and immersed in water overnight. The resulting yellowish solid product was filtered, and dried under vacuum at room temperature for 24 h. FTIR (KBr): ν_{max} = 3434, 2925, 1637, 1587, 1509, 1452, 1240, 1171, 1107, 1027, 802, 753 cm^{-1}; ^{13}C NMR (Solid state, 100 MHz) δ: broad unresolved peaks at 159.22, 151.70, 132.38, 114.44, 72.31, 43.00, 38.21; elemental analysis: found C, 59.70; H, 5.82; N, 5.25 %.

4.3.5 Network swelling study

Fully dried network sample was weighed and equilibrated in distilled water at 25 ^{o}C for 48h. The equilibrium swelling capacity or swelling ratio (*Q*) was calculated as follows: $Q = W_0 / W_d$; Where, W_0 is the weight of water in the swollen network and W_d is the dry weight of the network. The swelling studies were repeatedly performed by thrice with 5% standard deviation.

4.3.6 Adsorption experiments

The batch adsorption studies were performed by adding pre-weighed amount of sorbents to the azo-dye solution with predefined initial concentration at different pH values of 2.30, 7.20 and 10.96 and shaken at room temperature. The pH was adjusted to a given value using either 1M NaOH or 1M HCl solutions. Aliquots were periodically withdrawn from the solutions and the remaining concentrations of azo dyes were measured by UV-vis spectrophotometer at the maximum absorptions. The amount of dye adsorbed (mg/g) at equilibrium (q_e) and at time t (q_t) were calculated by using the formulae:

$$q_t = \frac{(C_0 - C_t)V}{W} \quad ; \quad q_e = \frac{(C_0 - C_e)V}{W}$$

where C_0, C_t and C_e represent the initial, t time and equilibrium liquid-phase concentrations of azo-dye (mg/L), respectively. V is the volume of dye solution (L) that was taken and W is the weight of the adsorbent (g). Freundlich isotherm model[4.2,4.3] was used to describe the adsorption equilibrium.

The linearized form of the Freundlich equation is given as follows:

$$\ln q_e = \ln K_f + 1/n \ln C_e$$

where K_f and n are Freundlich constants related to sorption capacity and sorption intensity, respectively. K_f and 1/n were obtained from the plot of $\ln q_e$ *vs*. $\ln C_e$.

4.3.7 Desorption and reusability study

After completion of first adsorption cycle, azo-dye loaded adsorbent was recovered and kept in dil H_2SO_4 solution (8.0 N). The mixtures were shaken at 25^oC for a period of 24h to desorb azo dyes (MO/OII/OG). The adsorbed azo dye desorbed was quantified using UV-vis spectrophotometer. Desorption amount was calculated using the following equation.

$$\text{Desorption (\%)} = \frac{(C_{des} \times V_{des})}{(C_0 - C_e)\, V_{ads}} \times 100$$

Where V_{des} = volume of desorbent used,

C_{des} = final concentration of azo dye in solution after desorption

Thereafter, the regeneration process of adsorbent was performed by putting it in water with pH adjustment to neutral with dilute NaOH solution. The resulting regenerated sorbent was filtered, dried and reused in the next cycle. The adsorption/desorption process was repeated three times.

4.4 Results and discussion

4.4.1 Synthesis and characterization

Novolac epoxy resin **2.2** bearing reactive epoxy functionality deserves particular attention as crosslinkable precursor to cure with a variety of ligating agents, in particular, amine molecules. Pyridine and its derivatives are well known ligands in coordination chemistry due to their basicity and nonhydrolyzability. Thus incorporation of such ligating molecules tends to be an innovative strategy to design new novolac-based adsorbents. The route followed for the synthesis of novolac-based network **4.1** is shown in Scheme 4.1. It was prepared in a similar manner as illustrated in *Chapter-2*. The crosslinking reaction between novolac epoxy resin precursor **2.2** and 3-aminopyridine gave the network **4.1** in good yield. The presence of aminopyridine units in combination with other functional groups such as hydroxyl and ether in the resulting network seems to have a capacity to interact by physical and chemical forces in the adsorption of wide variety of azo-dye molecules.

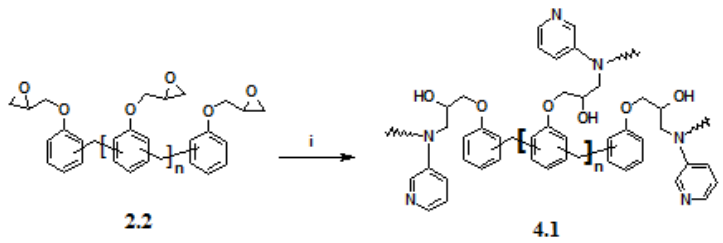

Scheme 4.1. Synthesis of **4.1** (i) 3-Aminopyridine, 1,4-dioxane/methanol, heat

Furthermore, multiple characteristics of novolac type phenolic resin, e.g., chemical resistance, dimensional stability, low-cost, branched structure deserve particular attention in dye adsorption monitoring.

The obtained network **4.1** was characterized by FTIR, ^{13}C NMR, elemental, FESEM, BET, thermal (TGA) and paticle size analyses. The FTIR spectrum of **4.1** (Figure 4.2) showed the broad absorption band in the region 3414 – 3449 cm^{-1}, which is indicative of the existence of O-H and N-H moieties. The band observed at 2925 cm^{-1} is assigned to the aliphatic C–H stretching. Two absorption bands at 1634 and 1587 cm^{-1} were observed, corresponding to aromatic ring skeleton stretching vibrations and a combination of N-H bending and pyridine ring (C=N) stretching vibrations. The presence of the aminopyridine units was further substantiated with the appearance of C–N stretch band at 1339 cm^{-1}. Remaining vibrational modes are listed in experimental section.

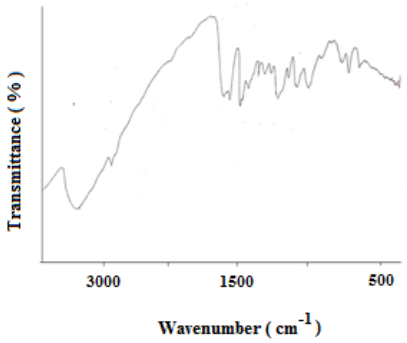

Figure 4.2 FTIR spectrum of **4.1**

The solid state ^{13}C NMR spectral examination (Figure 4.3) further verified the structural integrity of **4.1**. The broad signals located at 159.81, 151.36, 133.15 and 114.78 ppm were assigned to the aromatic carbons of novolac skeleton and pyridine units. The signals appeared at 72.82 and 38.21 ppm was attributed to the aliphatic carbons of network. The weight percent nitrogen content in elemental analysis further confirms the presence of aminopyridine units.

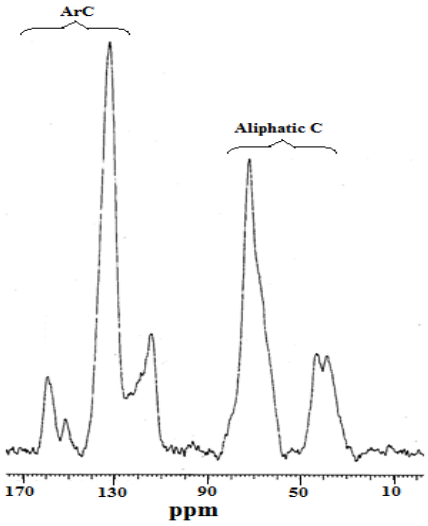

Figure 4.3 solid state ^{13}C NMR spectrum of **4.1**

The morphology of **4.1** was examined by FESEM. As shown in Figure 4.4a, the porous surface morphology of **4.1** can be clearly seen. The magnified image (Figure 4.4b) further provided clearer view of the morphology with well-developed pores. The presence of porous structure in combination with rich functionalities would potentiate its suitability for azo-dye trapping and adsorption.

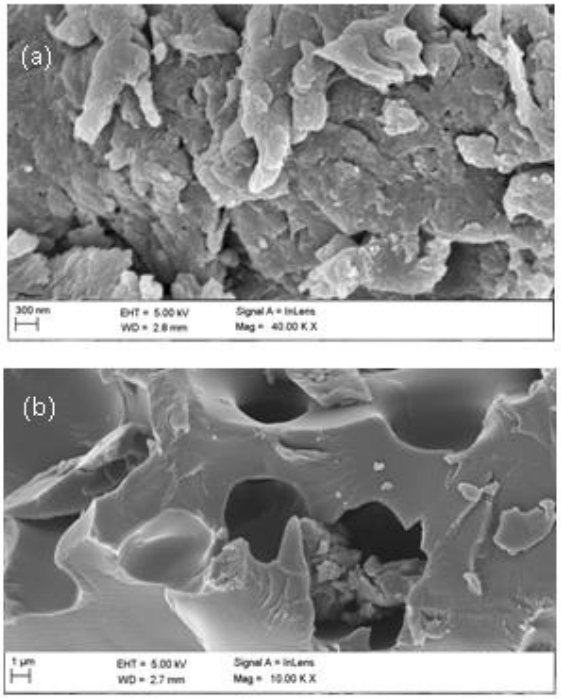

Figure 4.4 FESEM images of **4.1.**

Thermal behavior of **4.1** was investigated by TGA and the results are summarized in Table 4.1. The network is thermally stable up to a 15% weight loss temperature of approximately 278 ^{o}C, which may be attributed to the loss of moisture and solvent trapped within the micropore structure. A three-step weight loss of **4.1** appearing at ~278 – 344 ^{0}C, ~344 – 444 ^{0}C and above 444 ^{0}C (Figure 4.5) can be attributed to the structural changes, such as loss of functional groups in association with decomposition of network backbone. The onset decomposition temperature (~278 ^{o}C) suggests also its applicability to treat high temperature wastewater.

Table 4.1. Thermal properties (TGA) of **4.1**

Network	T_d^{15}(°C)	Stage	Temp. range (°C)	Weight loss %	Y_c at 800°C (wt%)
4.1	278	1	278-344	23	
		2	344-444	27	21

TGA was performed at a heating rate of 10°C/min under nitrogen flow; T_d^{15} = Temperature at which 15% weight loss occurred; Y_c = char yield.

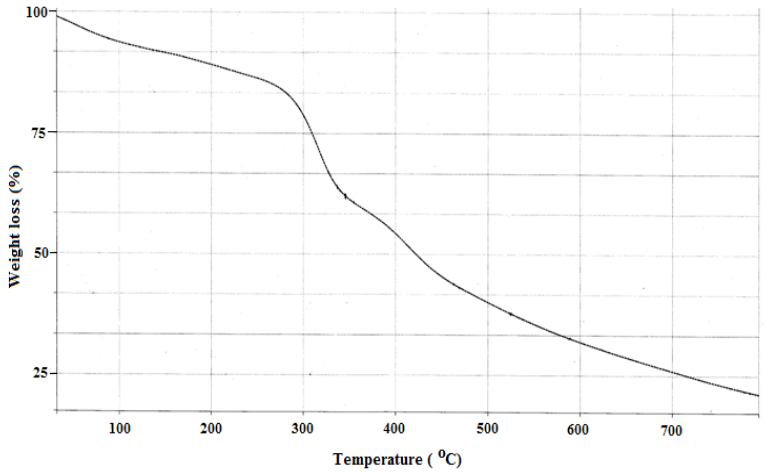

Figure 4.5 TGA Thermograme of **4.1**

The swelling behavior of **4.1** was studied in water. The network swells considerably and equilibrium was achieved within 48h. Significant swelling indicates the availability of hydrophilic sites to interact with water molecules promoting network expansion. This property was anticipated to encourage its applicability as sorbent material for hydrophilic azo dye molecules.

It was claimed that sorbent particle sizes influences adsorption behaviour[4.4]. This behaviour could be related to the surface area and the number of available binding sites of sorbent. It is suggested that smaller particles yield larger surface areas that are likely to render the dye uptake and removal efficiency. Thus, prior to evaluation of dye adsorption, the particle size of the sorbent network was measured. Figure 4.6 shows the particle features of network powder **4.1** in the range 10 − 238 μm with monomodal size distribution.

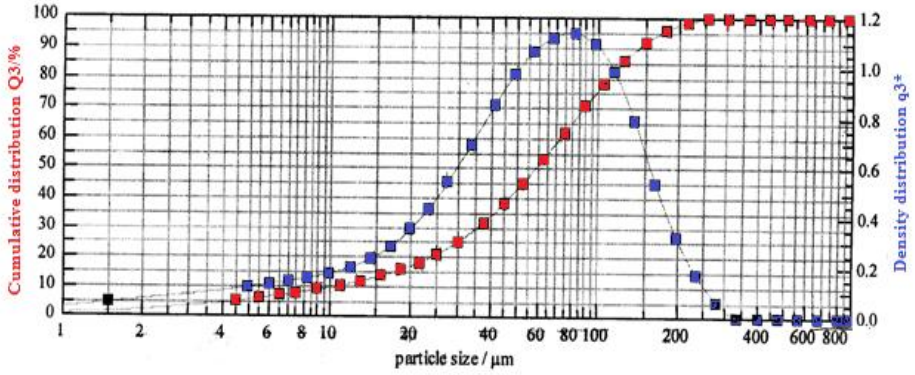

Figure 4.6 TGA Thermograme of **4.1**

The surface area of **4.1** was determined using standard nitrogen adsorption porosimetric technique employing BET method. Table 4.2 summarizes the BET parameters of network. The dye adsorption behavior could be predicted from surface area / pore volume and porosity information.

Table 4.2 BET parameters of **4.1**

Specific surface area (m^2/g)	Total pore volume (cm^3/g)
7.2702 ± 0.3000	1.670091

4.4.2 Azo dye adsorption studies

The popular azo dyes like methyl orange (MO), Orange-II (OII) and orange-G (OG) whose characteristics and chemical structures are illustrated in *Chapter-2* were employed as model dyes in the evaluation of adsorption performance of pyridine-rich network **4.1**. Azo dye adsorption was studied as a function of contact time at initial pH values of 2.30, 7.20 and 10.96.

The pH of the solution was reported[4.5-4.8] to present an important controlling parameter in the dye adsorption process because it affects the adsorbent surface charge and the degree of ionization of dye adsorbates. As determined spectrophotometrically, prompt decrease in absorption peaks of azo dyes due to adsorption as a function of time was noted. This quantified the amount of azo-dye molecules adsorbed onto **4.1**. Figure 4.7, for instance, shows the UV-vis absorbance decay of MO, OII and OG solutions at specified time intervals.

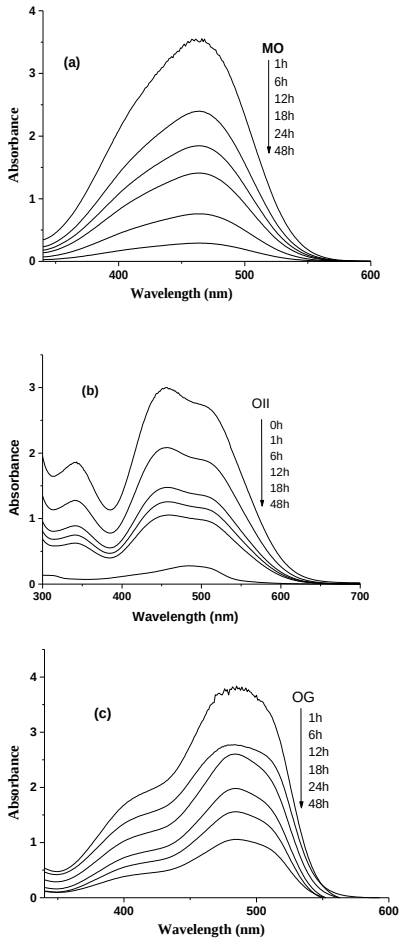

Figure 4.7. UV-vis spectral changes of the solutions of (a) MO (1.82 x 10^{-4}M; pH 7.20), (b) O II (4.28 x 10^{-4}M; pH 10.96) and (c) OG (3.31 x 10^{-4}M; pH 2.30) as a function of adsorption time for **4.1;** (temperature: 25^{o}C).

It was further noticed that sharp adsorption occurred at the beginning stage, followed by gradually decrease approaching equilibrium within 48h. Figure 4.8 presents the adsorption of MO, OII and OG onto **4.1** as a function of the adsorption time, studied with different pHs. The pattern of graphs was almost

same for all dyes examined. The initial rapid adsorption was probably due to the abundant availability of the vacant sorption sites. However, very slow adsorption at the later stages is probably attributed to the slow pore diffusion of the dyes into the bulk of the sorbent networks. The maximum adsorption at the beginning appears to be advantageous with respect to the reduction of reactor volumes and times.

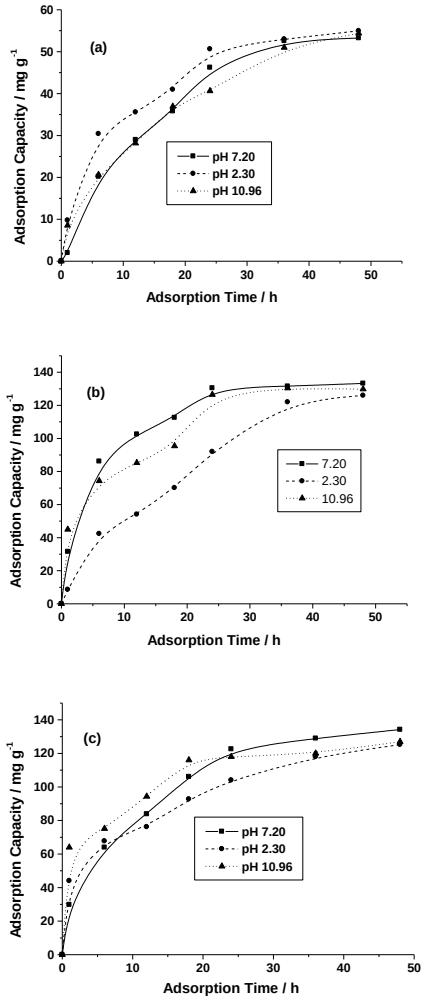

Figure 4.8 Time profile for azo-dye adsorption on **4.1** at different pH (a) MO adsorption (C_0 = 60 mg L^{-1}; 1.82 x 10^{-4}M); (b) O II adsorption (C_0 = 150 mg L^{-1}; 4.28 x 10^{-4}M); (c) OG adsorption (C_0 = 150 mg L^{-1};3.31 x 10^{-4}M.

Figure 4.9 presents the relationship between the initial solution pH on the equilibrium adsorption capacity of **4.1**. The results revealed no notable difference in achieving maximal adsorption (q_e, mg/g) at the tested pH range. Generally, high pH value (basic condition) inhibits the adsorption of anionic dyes[4.9]. But such a good adsorption efficacy of **4.1** toward azo dyes at the basic pH, as presented in Figure 4.9, is also interesting and confirms its additional merit. Thus, the effective adsorption at the extended operational pH range (acidic-neutral-basic conditions) could ensure the practical utility of the designed sorbent in the treatment of industrial dyeing-wastewaters having a wide range of initial pH values. Furthermore, more effective adsorption of OII and OG compared to MO at this pH range indicates more affinity towards the active sites of **4.1**.

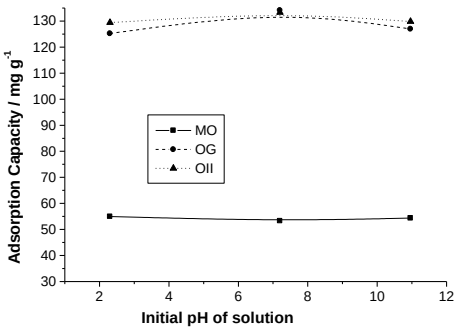

Figure 4.9 Effect of solution pH on the adsorption capacity of **4.1** for 48h of contact time [MO adsorption (C_0 = 60 mg L^{-1}; 1.82 x 10^{-4}M); O II adsorption (C_0 = 150 mg L^{-1}; 4.28 x 10^{-4}M); OG adsorption (C_0 = 150 mg L^{-1};3.31 x 10^{-4}M); 25^{o}C].

Freundlich isotherm model was applied to assess the performance of adsorption process of representative azo dyes onto adsorbent **4.1**. The linear fit to the plots of ln q_e *vs*. ln C_e in this isotherm model yields Freundlich constants. The slope and intercept of each linear fit was used to calculate the values of Freundlich constants (Figures 4.10, 4.11, 4.12). The graphically calculated isotherm parameters along with the correlation coefficients (R^2) are listed in Table 4.3. The values of K_f are indicative of good adsorption capacity of **4.1**. On the other hand, the values of n are in the range ($10 > n > 1$)[4.6,4.9-4.11] indicating the favorability of adsorption process. The correlation ($R^2 > 0.96$) suggested the well fitting of Freundlich isotherm model to the experimental data.

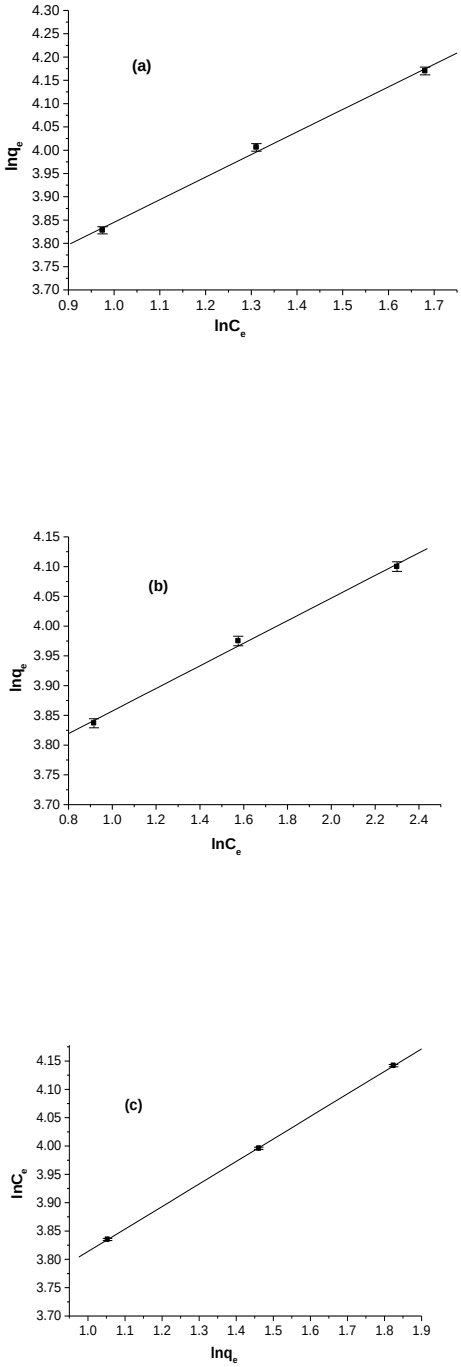

Figure 4.10 The fittings of adsorption isotherm data to Freundlich model for the adsorption of MO onto **4.1** at (a) pH 2.30, (b) pH 7.20 and (c) pH 10.96 at 25ºC

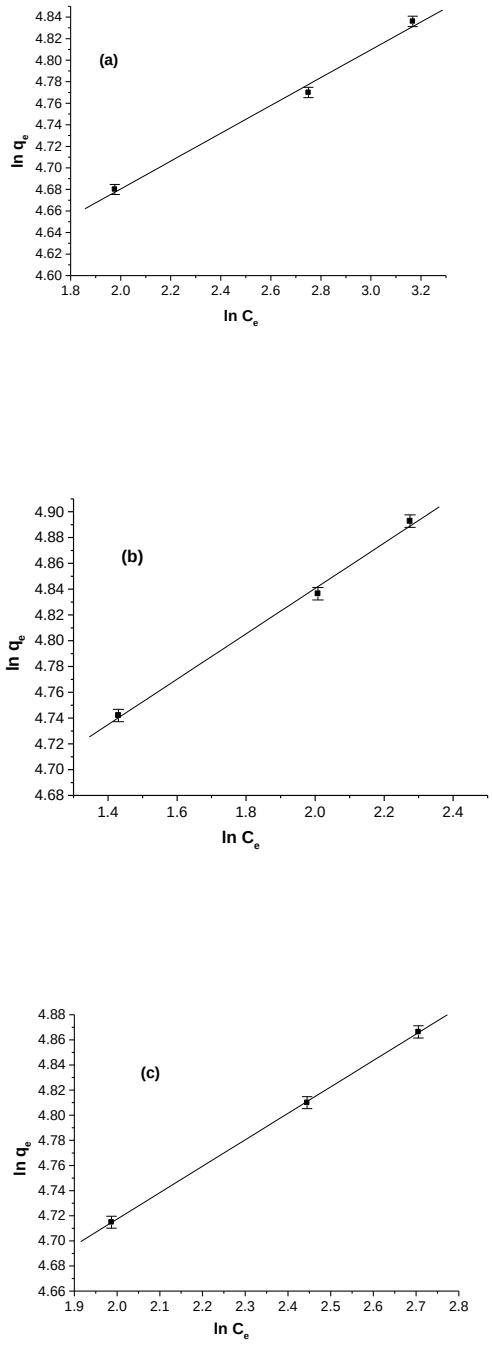

Figure 4.11 The fittings of adsorption isotherm data to Freundlich model for the adsorption of OII onto **4.1** at (a) pH 2.30, (b) pH 7.20 and (c) pH 10.96 at 25^{o}C

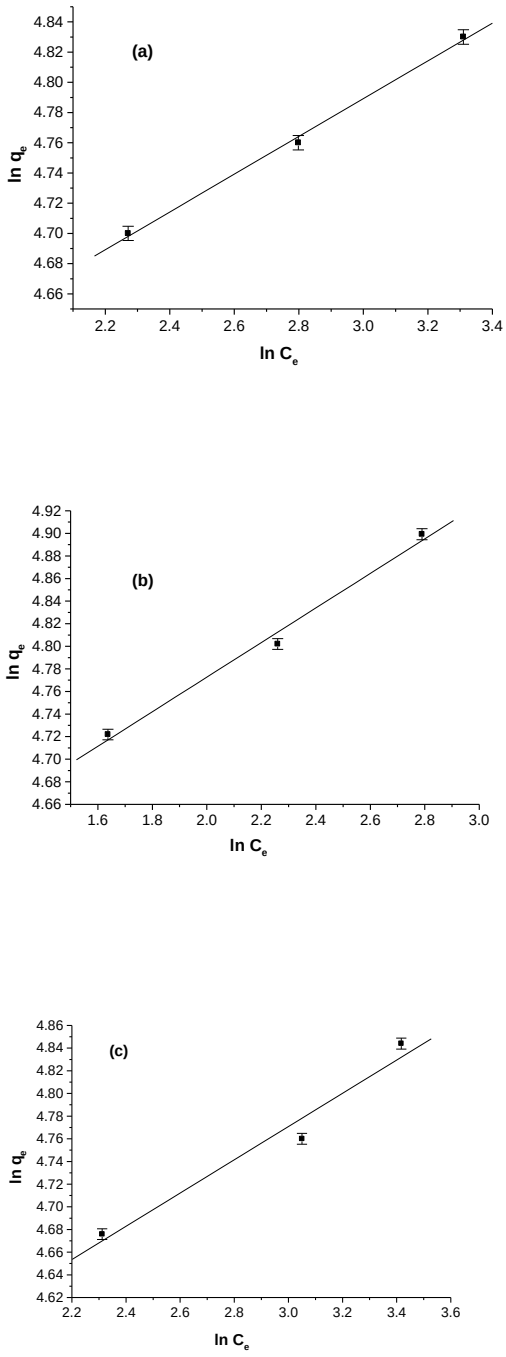

Figure 4.12 The fittings of adsorption isotherm data to Freundlich model for the adsorption of OG onto **4.1** at (a) pH 2.30, (b) pH 7.20 and (c) pH 10.96 at 25^{o}C

Table 4.3 Adsorption isotherm parameters of Freundlich model for MO, OII and OG sorptions onto **4.1** at 298 K.

Azo-dye	pH	Freundlich Isotherm			
		K_f	1/n	n	R^2
MO	2.30	28.822	0.4844	2.064	0.9974
	7.20	39.151	0.1898	5.267	0.9968
	10.96	30.447	0.3976	2.515	0.9999
O II	2.30	83.275	0.1291	7.742	0.9931
	7.20	88.978	0.1760	5.679	0.9958
	10.96	73.429	0.2105	4.750	0.9999
OG	2.30	82.611	0.1250	7.998	0.9971
	7.20	87.047	0.1531	6.531	0.9895
	10.96	76.030	0.1465	6.823	0.9638

FTIR spectra further provided qualitative evidence on the interactions between **4.1** and azo-dyes. Comparison of FTIR spectra before and after azo dye adsorption exhibited the appearance of broad and fine structured band in the region 3414 – 3449 cm^{-1} (O-H and N-H stretch). Meanwhile, the absorption band of neat **4.1** at 1587 cm^{-1} (N-H bend and pyridine ring C=N stretch) shifted to higher wavenumber ($\Delta\nu$ = 28-30 cm^{-1}) on azo dye adsorption. An increase in intensity of this band was also noted. Bands of dye loaded network, located at 1172 and 1028 cm^{-1}, were linked to the asymmetric and symmetric stretching of azo dye SO_3^- groups. The assigned bands are at lower wavenumber ($\Delta\nu$ = 8-12 cm^{-1}) in comparison with pure azo dye molecules. Based on these evidences, it can be concluded that the interaction exist between network functionalities and azo dye molecules.

The salting-out agents (especially sodium chloride), often present in industrial dyeing-effluents, may have influence on dye removal ability[4.12-4.15]. Thus, in view of practical applicability, it is necessary to investigate the dye uptake capacity of **4.1** in presence of sodium chloride. It is worth to note that

the equilibrium adsorption of azo dyes was hardly influenced by NaCl (0.1 M). This finding points to the network-dye interactions, essentially independent of salting-out effect.

It was also observed that the yellow colored sorbent **4.1** gradually changed to red with concomitant color reduction of dye solutions after the adsorption process (Figure 4.13). This visual observation signified the successful coverage of sorbent surface with dye molecules. Figure 4.14 reports the color change of dye solutions when exposed to **4.1** for 48h revealing dye concentration reduction due to adsorption.

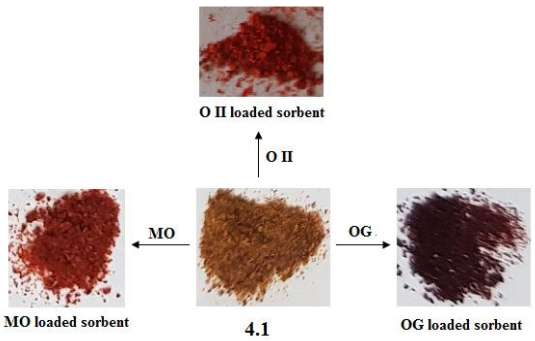

Figure 4.13 Photo showing color change of **4.1** on adsorption of azo dyes for 48h.

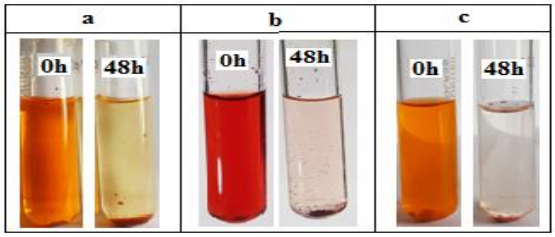

Figure 4.14 Photo image of adsorptive separation of azo dyes using sorbent **4.1** (a) MO adsorption (C_0 = 60 mg L^{-1}; pH 7.20) (b) O II adsorption (C_0 = 150 mg L^{-1}; pH 10.96) (c) OG adsorption (C_0 = 150 mg L^{-1}; pH 2.30); 25ºC.

4.4.3 Desorption and reusability study

Reusability of adsorbent with dye recovery is also of important concern for its practical application. It was found that more than 90% azo dyes get readily desorbed from **4.1** when desorption experiment was carried out in dil H_2SO_4 solution. However, removal efficiency of the regenerated sorbent was still over 80% after three consecutive runs. The recycling potential makes the sorbent **4.1** economically attractive in the treatment of azo-dye colored polluted waters.

4.4.4 Adsorption-Desorption Mechanism

On the basis of author's reports given in *Chapter-2* with cited references and experimental observations, the proposed mechanism for dye adsorption and desorption is outlined in Figure 4.15. The effect of pH on the adsorption performance of **4.1** is different from that of our previously reported novolac-

based adsorbents given in *Chapter-2*, which exhibited drastic drop in adsorption at alkaline pH. Dye adsorption at basic pH, clearly, is quite significant for the present material. Presumably, pyridyl groups induce complex process of interactions with dye molecules in combination with other interacting motifs (amino, hydroxy and ether functionalities) of the network[4.16-4.19]. In the acidic (pH = 2.30) to nearly neutral region (pH = 7.20) the pyridine units in combination with other motifs of the sorbent are responsible for azo dye adsorption. At lower pH, the sorbent surface becomes positively charged due to the protonation of pyridine nitrogen favoring both electrostatic and hydrogen bonding interactions with sulphonate groups ($–SO_3^-$) of azo dye molecules as illustrated in Figure 4.15. Also other motifs of the sorbent get involved in hydrogen bonding interactions (N-H---$^-O_3S–$ and –O-H---$^-O_3S–$). The density of positive charges on the network is gradually lessened with pH increase due to deprotonation of pyridinium ion, which probably creates an effective organic environment. This is believed to intensify the physical forces (hydrophobic, π-π stacking, hydrogen bonding) only participated in the adsorption process. Further, the attractive physical forces between the adsorbent and the anionic organic dyes at higher pH (basic condition) might be dominant disfavoring the adsorption of competing OH^- ions. However, the adsorption of OG/OII by **4.1** is higher than MO attributing to the presence of more number of functional groups and extra π-surface in OG/OII structures.

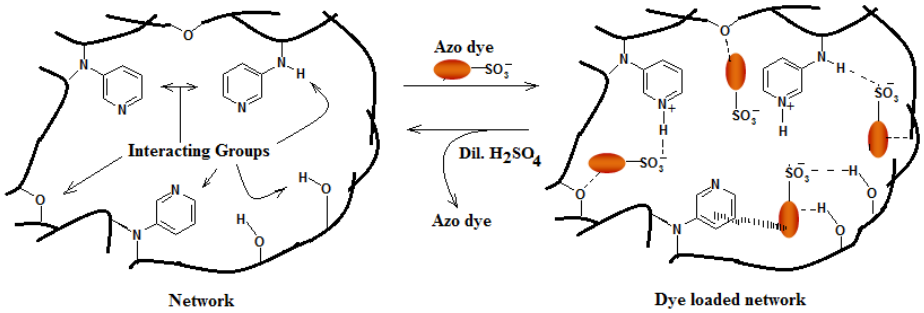

Figure 4.15 A proposed mechanism of adsorption: Attractive interactions (electrostatic attraction, hydrogen bonds and π-π stacking) occurring within the network polymer matrix.

4.4.5 Comparison of adsorption performance

The comparison of adsorption capacity with a few other reported adsorbents is summarized in Table 4.4 to demonstrate the importance of **4.1** used in this work. No information is available in the literature on azo dye adsorption capacities of other adsorbents at pH > 7.0 to compare with our findings. It can be seen from this table that the adsorption capacity of **4.1** at the extended operational pH range (acidic-neutral-basic conditions) is comparable or better than other reported adsorbents. The features of low cost, easy preparation, high stability, functional density and reusability are also coupled with the adsorption performance. Therefore, sorbent **4.1** revealed its potential to be

recommended as prominent candidate for the removal of azo dye colorants from water.

Table 4.4 Comparison of the equilibrium adsorption capacity of **4.1** with different adsorbents for some azo dyes at room temperature.

Adsorbents	Adsorbates	q_e (mg g^{-1})	pH
Modified wheat straw[4.20]	MO	50.4	3.0
Multiwalled carbon nanotubes[4.21]	MO	52.86	2.3
Organic copolymer of triptycene and crown-ether-15[4.22]	MO	64.8	6.0
Surfactant-coated Zeolite[4.23]	OII	38.96	1.0
Novolac resin-based network with aminopyridine units (present study)	MO	54.97	2.3
		53.25	7.2
		54.38	10.96
	OG	125.21	2.3
		134.2	7.2
		127.0	10.96
	OII	126.0	2.3
		133.33	7.2
		130.37	10.96

4.5 Conclusion

This chapter describes the synthesis of network polymer **4.1** using easily accessible novolac-based epoxy resin as a precursor. 3-aminopyridine served

as cross-linking agent in this network. The characterization of **4.1** was performed with: FTIR, solid state ^{13}C NMR, FESEM, BET, thermal (TGA), elemental and particle size analyses. The network was evaluated in the adsorptive removal of selected MO, O II and OG azo dyes from aqueous media where the effect of various parameters including solution pH, contact time and initial dye concentration were investigated. The results suggested that more functionalities/π-surface of OG/OII structure favor higher adsorption than MO. The influence of pH on adsorption of azo dyes was studied. Both electrostatic interaction and physical forces are proposed to be involved in the adsorption mechanism of azo dyes onto **4.1**. Compared to the reported adsorbents in Chapters 2 and 3, the obtained network turned out to be admirable adsorbent for removal of azo dyes (MO/OII/OG) over a wide pH range, which is crucial for field use of wastewater treatment. Equilibrium adsorption data appears to fit Freundlich isotherm model. The result revealed the typical physical process of adsorption ($n > 1$). FTIR studies provide information on sorbent functional sites participating in dye binding process. Moreover, the recycling potential of **4.1** is indicated from convenient desorption and reusability experiments. This work demonstrates that **4.1** is a cost-effective, recyclable adsorbing material for azo dye pollutants and may have great potential for applications in water remediation.

4.6 Further scope of work

The author recommends further research:

i) Further research to investigate the adsorption capacities of such adsorbing network material toward a variety of azo dye colorants is required.

ii) For practical application, the potential of such adsorbent for removal of azo dye colorants from real wastewater samples needs further studies.

iii) It is additionally recommended for the development of varieties of novolac-based network materials manipulating the adsorption properties and broadening the application potential.